INTERNATIONAL JOURNAL FOR NUMERICAL METHODS IN FLUIDS
Int. J. Numer. Meth. Fluids 2007; **53**:277–304
Published online 6 July 2006 in Wiley InterScience (www.interscience.wiley.com). DOI: 10.1002/fld.1292

Numerical modelling of complex turbulent free-surface flows with the SPH method: an overview

D. Violeau*,† and R. Issa

EDF R&D/Laboratoire National d'Hydraulique et Environnement, 6 quai Watier, 78400 Chatou, France

SUMMARY

The gridless smoothed particle hydrodynamics (SPH) method is now commonly used in computational fluid dynamics (CFD) and appears to be promising in predicting complex free-surface flows. However, increasing flow complexity requires appropriate approaches for taking account of turbulent effects, whereas some authors are still working without any turbulence closure in SPH. A review of recently developed turbulence models adapted to the SPH method is presented herein, from the simplistic point of view of a one-equation model involving mixing length to more sophisticated (and thus realistic) models like explicit algebraic Reynolds stress models (EARSM) or large eddy simulation (LES). Each proposed model is tested and validated on the basis of schematic cases for which laboratory data, theoretical or numerical solutions are available in the general field of turbulent free-surface incompressible flows (e.g. open-channel flow and schematic dam break). They give satisfactory results, even though some progress should be made in the future in terms of free-surface influence and wall conditions. Recommendations are given to SPH users to apply this method to the modelling of complex free-surface turbulent flows. Copyright © 2006 John Wiley & Sons, Ltd.

Received 12 January 2006; Revised 27 April 2006; Accepted 27 April 2006

KEY WORDS: SPH; turbulence; k–ε model; EARSM; LES; gridless methods

1. INTRODUCTION

At the end of the 1970s, the smoothed particle hydrodynamics (SPH) numerical method was invented to simulate astrophysical problems, for which a meshless formalism is helpful, as pointed out by Gingold and Monaghan [1]. SPH is a fully Lagrangian method, which means that no computational mesh or grid is required. At the beginning of the 1980s, this method was successfully applied to other fields of computational physics [2], in particular for rapid dynamic phenomena

*Correspondence to: D. Violeau, EDF R&D/Laboratoire National d'Hydraulique et Environnement, 6 quai Watier, 78400 Chatou, France.
†E-mail: Damien.violeau@edf.fr

Contract/grant sponsor: EU commission; contract/grant number: HPMT-CT-01-00369

in solid [3] and fluid dynamics [4]. Today, SPH is becoming one of the most popular meshless methods for fluid dynamics and is commonly applied to real free-surface flows. The complete standard SPH equations are here presented in Section 2 and an example is presented and validated in Section 4 under laminar conditions.

However, literature regarding turbulence modelling in SPH has been quite scarce until now. Recently, the authors successfully applied mixing length [5, 6] and k–ε [7] models to a turbulent free-surface channel. A 3D large eddy simulation (LES) model was also applied to the collapse of a water column in a tank [8], while Shao and Gotoh [9] as well as Dalrymple and Rogers [10] applied a two-dimensional LES model to wave propagation and interaction with coastal defence. Given these promising developments, we present here a brief overview of the SPH tools and applications in computational fluid dynamics (CFD) for turbulent incompressible free-surface flows. We will include in our presentation a review of available SPH turbulent models based on transport equations, and try to highlight the advantages and drawbacks of each. The natural conservation properties of the SPH method will be presented in Section 3, and their consequences will be discussed. Staring from these considerations, we will first present turbulent closures based on transport equations like the well known k–ε model (Sections 5 and 6), with validations showing its advantages and limitations in the case of free-surface flows. An explicit algebraic Reynolds stress model (EARSM) is then proposed in Section 7, and his benefits are shown, while LES is presented in Section 8. Advantages and drawbacks of each model will be highlighted.

Our presentation will be supported by applications on schematic cases for which theoretical solutions or experimental data are available. For practical reasons related to computational cost, most of the presented application cases are two-dimensional (except in Section 8); however, the reader should keep in mind that the presented equations are also valid in three dimensions. On a theoretical point of view, emphasis will be placed on the conservativity properties of the proposed formulations.

2. THE SPH GOVERNING EQUATIONS

In this section, we briefly present the main ideas of SPH considering the specific field of fluid dynamics; for more details the reader can refer to References [2, 11]. The SPH formalism is based on the idea that a flow can be considered as a set of bulk parts of moving fluid referred to as 'particles'. Each particle a, located at $\mathbf{r}_a$, has a constant mass m_a and carries a density ρ_a, a pressure p_a, velocity vector $\mathbf{u}_a$, dynamic (respectively, kinematic) viscosity μ_a (respectively, $\nu_a = \mu_a/\rho_a$), and more generally different physical quantities if it is required (e.g. temperature or energy). All these quantities evolve according to governing equations, which are written in terms of *fluxes* between particles. At the heart of SPH, any function A of position $\mathbf{r}$ is written as a convolution product with an interpolant kernel function w_h:

$$A(\mathbf{r}) = \int_\Omega A(\mathbf{r}')w_h(\mathbf{r} - \mathbf{r}')\,\mathrm{d}r' + O(h^2) \tag{1}$$

The summation is extended to the entire domain Ω and the parameter h, namely the smoothing length, will be discussed later. Note that Equation (1) would be mathematically exact if the Dirac distribution $\delta(\mathbf{r} - \mathbf{r}')$ was written in place of w_h. The transition to a discrete domain is achieved

DOI: 10.1002/fld

by approximating (1) with a Riemann summation or by using the Monte-Carlo formula:

$$A(\mathbf{r}) = \sum_b \frac{m_b}{\rho_b} A(\mathbf{r}_b) w_h(\mathbf{r} - \mathbf{r}_b) + O(h^2) \tag{2}$$

where b is a dummy subscript referring to each particle present in the domain, the infinitesimal volume $\mathrm{d}r'$ being replaced by the volume m_b/ρ_b of particle b. Finally, assuming that the SPH approximation (2) is exact (i.e. neglecting the terms of order h^2) and considering the case of a spherical kernel (i.e. w_h only depends on the distance between particle pair), we can write the value of A at the location of particle a as

$$A(\mathbf{r}_a) = \sum_b \frac{m_b}{\rho_b} A_b w_h(r_{ab}) \tag{3}$$

where A_b is the value of A at the location $\mathbf{r}_b$ of particle b and r_{ab} denotes the distance between a and b. Equation (3) is called the SPH interpolation. It appears that (3) is differentiable, provided the kernel is differentiable too; if the function A corresponds to a scalar field, the basic form of its gradient at particle a can then be obtained by taking the gradient of (3):

$$\nabla A(\mathbf{r}_a) = \sum_b \frac{m_b}{\rho_b} A_b \nabla_a w_{ab} \tag{4}$$

in which the symbolic expression ∇_a denotes the gradient of the kernel taken with respect to the co-ordinates of particle a, while $w_h(r_{ab})$ is written w_{ab} for simplicity. However, as in the finite element method, the gradient of a scalar field A can here be written in several ways, each one presenting specific properties. A common way for writing pressure gradient in SPH, for example, consists of inserting density into the gradient operator in the continuous formalism:

$$\frac{1}{\rho}\nabla p = \nabla\frac{p}{\rho} + \frac{p}{\rho^2}\nabla\rho \tag{5}$$

Then, approximating the right-hand side of Equation (5) with relation (4) yields an SPH form of the pressure force experienced by a:

$$\left(-\frac{1}{\rho}\nabla p\right)_a = -\sum_b m_b \left(\frac{p_a}{\rho_a^2} + \frac{p_b}{\rho_b^2}\right) \nabla_a w_{ab} \tag{6}$$

In contrast to the gradient form (4), Equation (6) is asymmetric with respect to a and b subscripts, which provides many advantages (see Section 3).

This can also be done for any differential operator such as the divergence of a vector field. Henceforth, the SPH formalism allows the possibility of estimating any differential operator by using the kernel, without using any computational grid. A usual kernel example is the fourth-order

DOI: 10.1002/fld

spline, used in most of the applications of the present work:

$$f(q)=\frac{\alpha_d}{h^d}\begin{cases}\left(\frac{5}{2}-q\right)^4-5\left(\frac{3}{2}-q\right)^4+10\left(\frac{1}{2}-q\right)^4 & \text{if } 0\leqslant q\leqslant 0.5\\ \left(\frac{5}{2}-q\right)^4-5\left(\frac{3}{2}-q\right)^4 & \text{if } 0.5\leqslant q\leqslant 1.5\\ \left(\frac{5}{2}-q\right)^4 & \text{if } 1.5\leqslant q\leqslant 2.5\\ 0 & \text{otherwise}\end{cases} \tag{7}$$

where q is defined as the ratio r_{ab}/h and d is the problem dimension (generally 2 or 3). Besides, $\alpha_d=\frac{96}{1199}\pi$ if $d=2$ and $\frac{1}{20}\pi$ if $d=3$ to ensure kernel normalization. An important feature of (7) is that w_h is designed with a compact support proportional to h, as shown in Figure 1. The smoothing length h is commonly proportional to the initial particle spacing δr, so that each particle interacts with a finite number of neighbour particles (see Figure 2). In SPH equations like (6), it means that the summation runs over a reduced number of particles b, keeping the number of operations

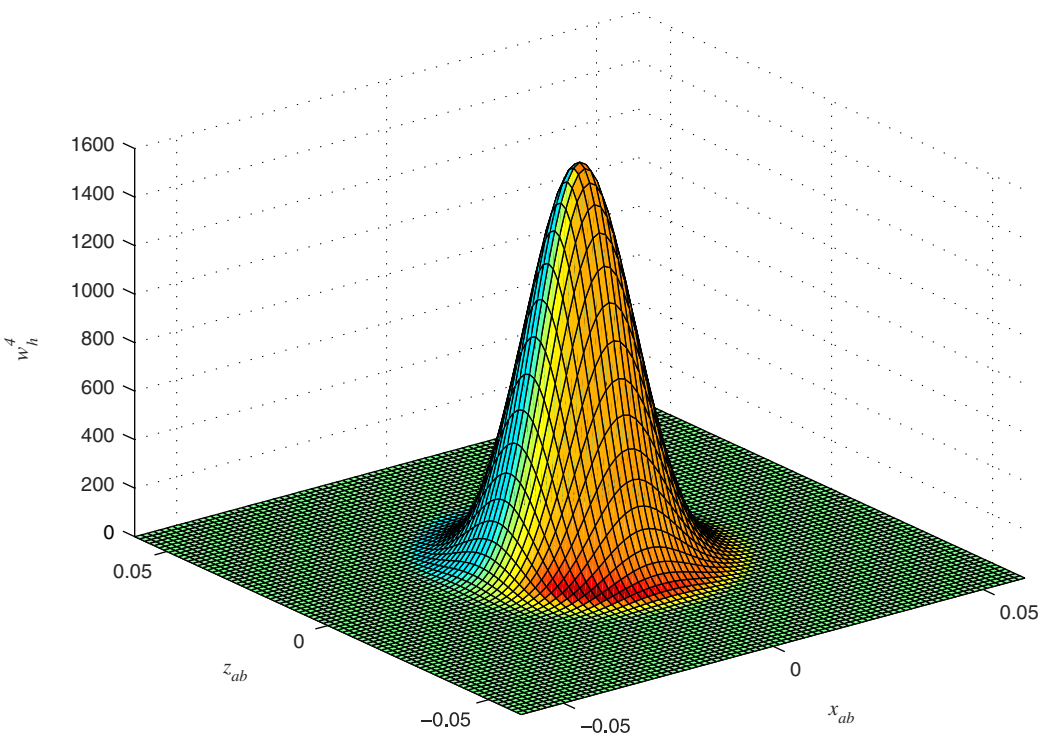

Figure 1. View of the fourth-order spline kernel in two dimensions.

DOI: 10.1002/fld

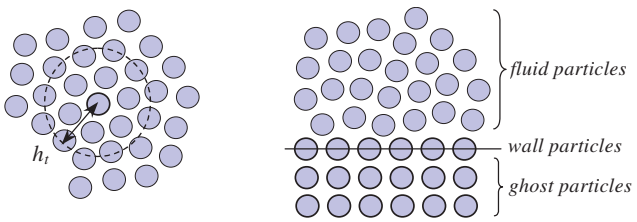

Figure 2. Left: particle interactions are commonly restricted to a finite neighbourhood bounded by a disc (respectively, a sphere) in 2D (respectively, in 3D). Right: wall and ghost particles are used to ensure a Neumann pressure condition on solid boundaries.

involved in the algorithm proportional to the particle number (for a given ratio $h/\delta r$). A link table between particles is thus established at each time step to keep the algorithm efficient.

Given these basic tools, the Navier–Stokes equations can be written in SPH formalism. The continuous Lagrangian form of these equations for a weakly compressible flow is

$$\frac{\mathrm{d}\mathbf{u}}{\mathrm{d}t} = -\frac{1}{\rho}\nabla p + \nu\nabla^2\mathbf{u} + \mathbf{g} \tag{8}$$

$$\frac{\mathrm{d}\rho}{\mathrm{d}t} = -\rho\nabla\cdot\mathbf{u} \tag{9}$$

where $\mathbf{g}$ is the acceleration of gravity (low density variations are assumed to have no effect in the momentum equation (8)). Given approximation (6) and applying similar considerations to the divergence and Laplace operators lead to a possible SPH form of (8) and (9) as

$$\frac{\mathrm{d}\mathbf{u}_a}{\mathrm{d}t} = -\sum_b m_b\left[\left(\frac{p_a}{\rho_a^2}+\frac{p_b}{\rho_b^2}\right)\nabla_a w_{ab} - \mathbf{\Pi}_{ab}\right] + \mathbf{g} \tag{10}$$

$$\frac{\mathrm{d}\rho_a}{\mathrm{d}t} = \sum_b m_b\mathbf{u}_{ab}\cdot\nabla_a w_{ab} \tag{11}$$

where $\mathbf{r}_{ab} = \mathbf{r}_a - \mathbf{r}_b$ and $\mathbf{u}_{ab} = \mathbf{u}_a - \mathbf{u}_b$. $\mathbf{\Pi}_{ab}$ is a viscous force presented in the literature in two main forms, one proposed by Monaghan [2]:

$$\mathbf{\Pi}_{ab} = 8\frac{\nu_a+\nu_b}{\rho_a+\rho_b}\frac{\mathbf{u}_{ab}\cdot\mathbf{r}_{ab}}{r_{ab}^2}\nabla_a w_{ab} \tag{12}$$

and the second one suggested by Morris *et al.* [11]:

$$\mathbf{\Pi}_{ab} = \frac{\mu_a+\mu_b}{\rho_a\rho_b}\frac{\mathbf{u}_{ab}}{r_{ab}^2}\mathbf{r}_{ab}\cdot\nabla_a w_{ab} \tag{13}$$

It has been shown in Reference [6] that both model the term $\nu\nabla^2\mathbf{u}$ of (8) and have specific properties, as shown in Section 3. Note that a small parameter is usually added to r_{ab}^2 in order to avoid zero denominators in (12) and (13); however, for simplicity it will be skipped in the following. Equation (10) is a momentum equation, used to compute particle velocity, while (11) is an SPH form of the continuity equation, giving particle density. Both can be integrated in time

DOI: 10.1002/fld

through traditional explicit numerical schemes (e.g. Euler or Runge–Kutta), and particle positions are obtained by velocity integration. Lastly, we need an estimation of pressure. For practical applications in the field of weakly compressible flows, Monaghan [4] suggested to estimate it from an equation of state:

$$p_a = \frac{\rho_0 c_0^2}{\gamma}\left[\left(\frac{\rho_a}{\rho_0}\right)^{\gamma} - 1\right] \tag{14}$$

in which ρ_0 is a reference density, c_0 a numerical speed of sound and $\gamma = 7$ for water. Then, if c_0 is high enough, Equation (14) is suitable for a weakly compressible fluid, which can model incompressibility with a sufficient accuracy. However, for numerical reasons, the value of c_0 in the model is not the true speed of sound; indeed, the time step is usually subject to some stability constraints:

$$\delta t = \min\left(0.4\frac{h}{c_0}, 0.25\min_a\left(\sqrt{\frac{h}{\gamma_a}}\right), 0.125\min_a\left(\frac{\rho_a h^2}{\mu_a}\right)\right) \tag{15}$$

where γ_a is the modulus of the acceleration of particle a. The first of these conditions is a Courant criterion; the coefficients are based on numerical experiments (see Reference [11]). The speed of sound appearing in the first constraint would yield very small time steps if one would set c_0 to its physical value; therefore, it is usually recommended to set it to an artificial (numerical) value equal to 10 times the maximum flow speed, keeping the relative density fluctuations less than 1%. With this approximation, SPH appears to be a weakly compressible method. It may be mentioned that pressure estimation from (14) is sometimes subject to instabilities and show scattered distributions [6]; in order to avoid these difficulties, some authors (e.g. Reference [9]) prefer solving a pressure Poisson equation. However, this approach implies additional numerical operations while the method based on a state equation remains quite simple; all the flows presented below were simulated using this approach, which is, according to Monaghan [4], a good balance between accuracy and simplicity for SPH.

Solid boundaries are often modelled with fixed wall particles and artificial repulsive forces [4], or alternatively with mirror particles [11]. We prefer the latter solution, since it keeps conservation laws valid (see Section 3). The main idea is to model walls with 'wall particles' (without any artificial repulsive force) and several layers of 'ghost particles' (see Figure 2, right picture), density of which is prescribed by symmetry when computing particle density through Equation (11). This means that when a mirror particle b contributes to the density evolution of a fluid particle a through the right-hand side of Equation (11), the same term is added to the density evolution of particle b. Thus, Equation (14) keeps pressure forces symmetric with respect to the wall, ensuring an artificial Neumann condition regarding pressure. Note that, in contrast to the method proposed in many SPH papers (e.g. Reference [11]), the presented algorithm is based on *fixed* ghost particles. This new pressure wall condition enables a perfect impermeability even in rapid dynamic phenomena such as dam breaking. Besides, contrary to the repulsive forces presented in Reference [3], the present formulation does not require any *ad hoc* coefficient. Under laminar conditions, wall and mirror particles have a zero velocity to prescribe a no-slip condition at the wall. In contrast, in our turbulent developments (Section 5), we will use the wall particles to prescribe Dirichlet or Neumann conditions of the modelled physical quantities.

DOI: 10.1002/fld

All the above-mentioned developments show that a strong advantage of the SPH method is the use of a Lagrangian formalism, for which advection terms are implicitly included in the particle time derivative (left-hand side of Equations (10) and (11)). One may also emphasize the fact that the present model and equations are equally valid in two and three dimensions, through the choice of an appropriate normalization constant in the kernel definition (7). The next section will examine additional advantages of SPH, in terms of conservation laws.

3. CONSERVATION PROPERTIES

As suggested in the previous section, the asymmetry of SPH equations with respect to a and b subscripts has a strong physical meaning. In this section, we will investigate this point, leading to some conclusions of interest for turbulence closures. In Equation (10), the quantity

$$m_a m_b \left[-\left(\frac{p_a}{\rho_a^2} + \frac{p_b}{\rho_b^2} \right) \nabla_a w_{ab} + \mathbf{\Pi}_{ab} \right] = \mathbf{F}_{b \to a} \tag{16}$$

is the force exerted by particle b on particle a, showing asymmetry with respect to a and b, regardless of the model used for viscous forces $\mathbf{\Pi}_{ab}$ (see Equations (12) and (13)). Indeed, the kernel gradient changes its sign when permuting a and b subscripts; hence the SPH form of fluid forces satisfies the action–reaction law:

$$\mathbf{F}_{b \to a} = -\mathbf{F}_{a \to b} \tag{17}$$

This immediately implies the conservation of total *linear* momentum for an isolated set of particles. More generally, the SPH equations have many interesting properties, among which they are Galilean-invariant. The above-mentioned features come from the fact that Equation (10) can be partially derived from an action principle (see Reference [12]). It is known that the basic equations of Lagrangian mechanics, coming from a variational principle, are the so-called Lagrange equations:

$$\frac{\mathrm{d}}{\mathrm{d}t} \frac{\partial L}{\partial \mathbf{u}_a} - \frac{\partial L}{\partial \mathbf{r}_a} = \mathbf{0} \tag{18}$$

for each particle a, L being a Lagrange function relative to the whole particle system, equal to the difference between kinetic and potential energies. Therefore, in SPH formalism, one can introduce an internal energy e_a for each particle, leading to

$$L = \frac{1}{2} \sum_b m_b \mathbf{u}_b^2 - \sum_b m_b e_b \tag{19}$$

Equation (18) then gives the equation of motion for particle a as

$$m_a \frac{\mathrm{d}\mathbf{u}_a}{\mathrm{d}t} = \sum_b m_b \frac{\partial e_b}{\partial \mathbf{r}_a} = \sum_b m_b \frac{\partial e_b}{\partial \rho_b} \frac{\partial \rho_b}{\partial \mathbf{r}_a} \tag{20}$$

DOI: 10.1002/fld

An estimation of the last term can be obtained from the SPH interpolation (3):

$$\frac{\partial \rho_b}{\partial \mathbf{r}_a} = \frac{\partial}{\partial \mathbf{r}_a} \sum_c m_c w_{bc} = m_a \nabla_a w_{ba} + \delta_{ab} \sum_c m_c \nabla_a w_{ac} \tag{21}$$

where δ_{ab} refers to Kronecker's notation. Thus, using the asymmetry of the kernel gradient, (20) gives

$$\frac{\mathrm{d}\mathbf{u}_a}{\mathrm{d}t} = -\sum_b m_b \left[\left(\frac{\partial e}{\partial \rho} \right)_a + \left(\frac{\partial e}{\partial \rho} \right)_b \right] \nabla_a w_{ab} \tag{22}$$

Eventually, the laws of thermodynamics show that internal energy (for non-dissipative media) satisfies the rule $\mathrm{d}e = -p\,\mathrm{d}V = (p/\rho^2)\,\mathrm{d}\rho$, so that p/ρ^2 is the derivative of internal energy with respect to the density. Changing $\partial e/\partial \rho$ with p/ρ^2 in (22) leads to the momentum equation (10) with pressure forces only (i.e. energy-conservative forces). This short demonstration shows that SPH is a very attractive method, based on strong physical considerations. One may emphasize the fact that various SPH forms for estimating pressure gradient are available, as in traditional mesh-based methods. The above-mentioned proof is mainly based on the assumption that the density should be written as in (21); Bonet and Lok [13] show that different approaches lead to various pressure gradient forms, all of them being asymmetric, thus conserving linear momentum and energy.

Shear (viscous) forces can also be accounted for by this approach, considering that fluid shear is a linear function of velocities (see Reference [14]), like in the Navier–Stokes momentum equation (8). The most general form of such a linear dependency for the viscous force experienced by a particle a can be written as

$$\mathbf{F}_a^{\mathrm{visc}} = -\sum_b \mathbf{A}_{ab} \mathbf{u}_{ab} \tag{23}$$

in which the $\mathbf{A}_{ab}$'s are second-order positive definite tensors, symmetric in a and b (which are *not* denoting tensor indices but particle labels). Equation (23) is a general SPH form of viscous forces; contrary to pressure forces, they do not appear as the derivative of a lagrangian function L with respect to positions $\mathbf{r}_a$, but as the derivative of a certain function F with respect to velocities $\mathbf{u}_a$. Indeed, one could possibly include them in the momentum equation (18) to yield

$$\frac{\mathrm{d}}{\mathrm{d}t} \frac{\partial L}{\partial \mathbf{u}_a} - \frac{\partial L}{\partial \mathbf{r}_a} + \frac{\partial F}{\partial \mathbf{u}_a} = \mathbf{0} \tag{24}$$

in which F is defined by the following quadratic form:

$$F = \frac{1}{2} \sum_{a,b} \mathbf{u}_{ab} \mathbf{A}_{ab} \mathbf{u}_{ab} \tag{25}$$

The physical meaning of F will appear further. Coming back to the forms given in Equation (10), we now see that $m_a m_b \boldsymbol{\Pi}_{ab} = -\mathbf{A}_{ab} \mathbf{u}_{ab}$. Furthermore, as a consequence of $\mathbf{A}$'s symmetry, the conservation of total linear momentum is preserved, as mentioned earlier. Let us show this result

DOI: 10.1002/fld

more properly. The time derivative of total momentum can be written as

$$\begin{aligned}\frac{\mathrm{d}}{\mathrm{d}t}\sum_a m_a\mathbf{u}_a &= \sum_a m_a\frac{\mathrm{d}\mathbf{u}_a}{\mathrm{d}t}\\ &= \sum_a\left(\frac{\partial L}{\partial \mathbf{r}_a}-\frac{\partial F}{\partial \mathbf{u}_a}\right)\\ &= \sum_{a,b}(\mathbf{F}^{\mathrm{pres}}_{b\to a}-\mathbf{A}_{ab}\mathbf{u}_{ab})\end{aligned} \tag{26}$$

where $\mathbf{F}^{\mathrm{pres}}_{b\to a}$ represents the part of forces from Equation (16) corresponding to pressure only. Thus, the properties of asymmetry of $\mathbf{F}^{\mathrm{pres}}_{b\to a}$ and $\mathbf{u}_{ab}$, together with the symmetry of $\mathbf{A}_{ab}$, show that the right-hand side of (26) vanishes. However, conservation of angular momentum turns differently. Using the asymmetry properties of the given variables, one finds

$$\begin{aligned}\frac{\mathrm{d}}{\mathrm{d}t}\sum_a \mathbf{r}_a\times m_a\mathbf{u}_a &= \sum_{a,b}\mathbf{r}_a\times(\mathbf{F}^{\mathrm{pres}}_{b\to a}-\mathbf{A}_{ab}\mathbf{u}_{ab})\\ &= \frac{1}{2}\sum_{a,b}\mathbf{r}_{ab}\times(\mathbf{F}^{\mathrm{pres}}_{b\to a}-\mathbf{A}_{ab}\mathbf{u}_{ab})\end{aligned} \tag{27}$$

Thus, it appears that the conservation of angular momentum of pressure forces is due to the fact that $\mathbf{F}^{\mathrm{pres}}_{b\to a}$, like $\nabla_a w_{ab}$, is co-linear with $\mathbf{r}_{ab}$ (see e.g. the right-hand side of Equation (22)). On the other hand, viscous forces conserve angular momentum only if $\mathbf{r}_{ab}\times(\mathbf{A}_{ab}\mathbf{u}_{ab})=\mathbf{0}$, which occurs if $\mathbf{A}_{ab}$ takes the general form

$$\mathbf{A}_{ab}=\mathbf{r}_{ab}\otimes\boldsymbol{\beta}_{ab} \tag{28}$$

where $\boldsymbol{\beta}_{ab}$ is a vector field satisfying $\boldsymbol{\beta}_{ab}=-\boldsymbol{\beta}_{ba}$. In this case, shear forces (23) can then be rewritten as

$$-\frac{\partial F}{\partial \mathbf{u}_a}=-\sum_b(\boldsymbol{\beta}_{ab}\cdot\mathbf{u}_{ab})\mathbf{r}_{ab} \tag{29}$$

The form written in (12) is then relevant, with the following choice:

$$\boldsymbol{\beta}_{ab}=-8m_am_b\frac{v_a+v_b}{\rho_a+\rho_b}|\nabla_a w_{ab}|\frac{\mathbf{r}_{ab}}{r^3_{ab}} \tag{30}$$

In contrast, the form (13) does not satisfy angular momentum conservation but has another property. Let us have a look at the general viscous term (23) in the particular case of a rigid body rotation:

$$-\frac{\partial F}{\partial \mathbf{u}_a}=-\omega\sum_b\mathbf{A}_{ab}(\mathbf{e}\times\mathbf{r}_{ab}) \tag{31}$$

where ω is an angular velocity and $\mathbf{e}$ the unit vector perpendicular to the plane in which the rotation takes place. It is then easy to show that these shear forces vanish (as required) if and only if

$$\mathbf{A}_{ab}=\alpha_{ab}\mathbf{I} \tag{32}$$

DOI: 10.1002/fld

where $\mathbf{I}$ is the unit tensor. Equation (13) is a particular form of (32) with

$$\alpha_{ab} = -m_a m_b \frac{\mu_a + \mu_b}{\rho_a \rho_b} \frac{\mathbf{r}_{ab}}{r_{ab}^2} \cdot \nabla_a w_{ab} \tag{33}$$

In the following, we will prefer the latter choice, given that angular momentum conservation is not essential for our applications. Finally, we now take a look at energy conservation in Lagrangian models: Equations (23) and (24) can be used to show (see Reference [14]) that the time derivative of the total energy E of a set of particles is given by

$$\frac{\mathrm{d}E}{\mathrm{d}t} = -F \tag{34}$$

Hence, F is simply the energy dissipation rate. This shows that energy loss in SPH is only due to viscous forces, as in continuous equations. Equation (34) will be of great interest in the context of turbulence modelling (see Section 5).

To end with conservation properties and in the perspective of turbulent closure models, let us consider the possibility of modelling a transport and diffusion of a scalar in SPH. Viscous forces (13) suggest a similar form for general diffusion processes, so that the advection–diffusion equation for a scalar field C could be written in SPH form as

$$\frac{\mathrm{d}C_a}{\mathrm{d}t} = S_{C,a} + \sum_b m_b \frac{K_a + K_b}{\rho_a \rho_b} \frac{C_{ab}}{r_{ab}^2} \mathbf{r}_{ab} \cdot \nabla_a w_{ab} \tag{35}$$

where C_a and K_a are, respectively, scalar concentration and dynamic diffusion coefficient corresponding to particle a, while $C_{ab} = C_a - C_b$ and S_C is a source term. Many authors proposed similar models (see e.g. Reference [15] for temperature conductivity). Again, the asymmetry of Equation (35) can be interpreted in terms of conservation: forgetting the source term, it comes that the quantity

$$m_a m_b \frac{K_a + K_b}{\rho_a \rho_b} \frac{C_{ab}}{r_{ab}^2} \mathbf{r}_{ab} \cdot \nabla_a w_{ab} = q_{C,a} \tag{36}$$

is the C-flux from b to a (if C is measured by unit mass). Then, the total amount of scalar is exactly conserved. These considerations will be of great interest for turbulent closure (see Section 5). Note that the C-flux vanishes between two particles carrying the same concentration.

4. APPLICATION TO A LAMINAR FLOW

Before coming to turbulent flows, it appears interesting to test the ability of SPH to simulate incompressible laminar flows, although it was presented by many authors (see e.g. Reference [11]). The test case presented here is a 2D periodic hill flow designed within an Ercoftac workshop [16]. It involves about 20 000 fluid particles driven by a horizontal propelling force updated in time to prescribe the correct flow rate. The Reynolds number, based on the hill height and the bulk velocity, is equal to 50, and there is no free surface, the upper boundary being a solid wall (hence, gravity is not considered here). The results, compared with finite volume simulations [16], show an excellent agreement in terms of velocities (see Figures 3 and 4). One of the key challenges of such a simulation is the recirculation pattern given in Figure 4. One may mention the fact that numerical

DOI: 10.1002/fld

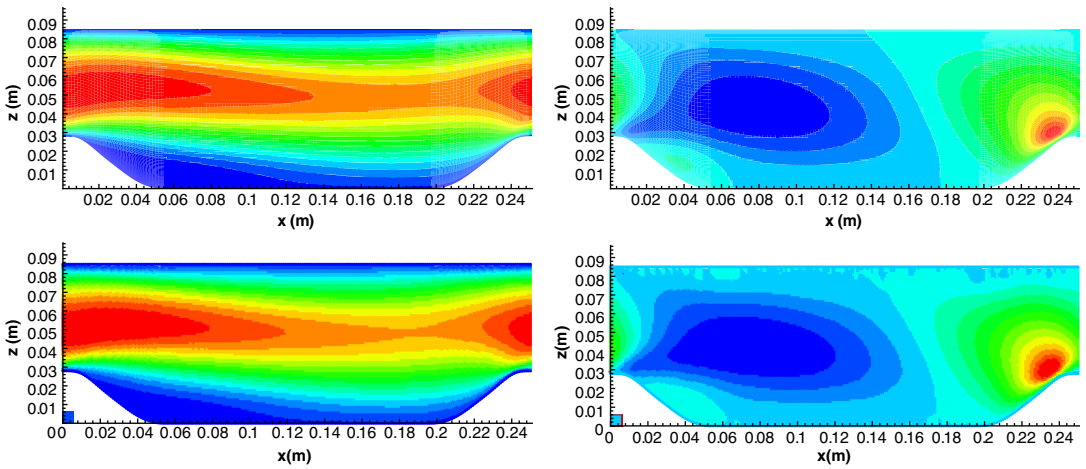

Figure 3. 2D laminar periodic hill flow simulated with a finite volume method (top) and with present SPH model (bottom). Axial (left) and vertical (right) velocities. The SPH velocity fields were time-averaged to reduce numerical fluctuations.

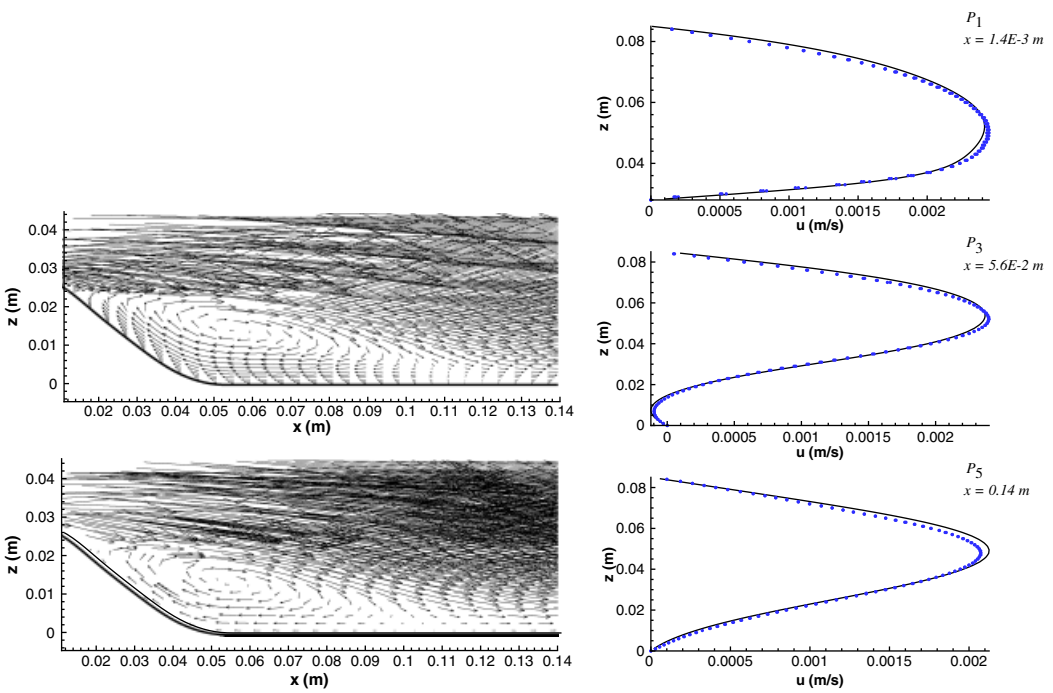

Figure 4. 2D laminar periodic hill flow simulated with a finite volume method (top left) and with present SPH model (bottom left). Velocity vectors in the recirculating area. Axial velocity profiles are presented on the right part; solid lines = finite volume method, symbols = present SPH model.

DOI: 10.1002/fld

fluctuations due to the SPH scheme occur in this case (in particular in the vicinity of the upper wall); thus the velocity fields presented in Figures 3 and 4 were obtained after time-averaging. Further information and data regarding the modelling of laminar flows with SPH are presented in References [6, 17].

5. TRADITIONAL TURBULENT CLOSURES

When considering turbulent flows, all physical quantities like pressures and velocities can be Reynolds-averaged, which is referred to by overstrike bars in the following. The Reynolds-averaged Navier–Stokes (RANS) momentum equation then takes the following form:

$$\frac{\mathrm{d}\overline{\mathbf{u}}}{\mathrm{d}t} = -\frac{1}{\rho}\nabla\overline{p} + \nu\Delta\overline{\mathbf{u}} - \frac{1}{\rho}\nabla\cdot(\rho\mathbf{R}) + \mathbf{g} \tag{37}$$

(from now on, terms like $\mathrm{d}/\mathrm{d}t$ refer to the Lagrangian derivative following the *mean* motion). If velocity turbulent fluctuations are denoted by a vector $\mathbf{u}'$, one can first assume that the Reynolds stress tensor $\mathbf{R} = \overline{\mathbf{u}'\otimes\mathbf{u}'}$ is modelled through the traditional Boussinesq eddy viscosity assumption, we write

$$\mathbf{R} = \tfrac{2}{3}k\mathbf{I} - 2\nu_T\mathbf{S} \tag{38}$$

where ν_T is an eddy viscosity, $k = \overline{u_i'u_i'}/2 = \mathrm{tr}(\mathbf{R})/2$ the turbulent kinetic energy and

$$S_{ij} = \frac{1}{2}\left(\frac{\partial\overline{u}_i}{\partial x_j} + \frac{\partial\overline{u}_j}{\partial x_i}\right) \tag{39}$$

are the components of the mean rate-of-strain tensor $\mathbf{S}$ (in contrast to indices a and b referring to particles, letters i and j here denote spatial co-ordinates). It is known that introducing (38) into (37) yields a momentum equation similar to the laminar one (8), the molecular viscosity being increased by the eddy viscosity. Considering formula (13) for modelling eddy viscous terms, the SPH momentum and continuity equations (10) and (11) can thus be rewritten as

$$\frac{\mathrm{d}\overline{\mathbf{u}}_a}{\mathrm{d}t} = -\sum_b m_b\left(\frac{\overline{p}_a}{\rho_a^2} + \frac{\overline{p}_b}{\rho_b^2} - \frac{\mu_{e,a}+\mu_{e,b}}{\rho_a\rho_b}\frac{\overline{\mathbf{u}}_{ab}}{r_{ab}^2}\mathbf{r}_{ab}\cdot\right)\nabla_a w_{ab} + \mathbf{g} \tag{40}$$

$$\frac{\mathrm{d}\rho_a}{\mathrm{d}t} = \sum_b m_b\overline{\mathbf{u}}_{ab}\cdot\nabla_a w_{ab} \tag{41}$$

with $\mu_{e,a} = \mu_a + \mu_{T,a}$. Therefore, each particle a is affected by a dynamic eddy viscosity, referred to as $\mu_{T,a} = \rho_a\nu_{T,a}$. Since we deal here with nearly incompressible flows, we assume that $\overline{\rho}_a \approx \rho_a$. The Reynolds-averaged pressure is still estimated using the previous equation of state (14). One may also add to the pressure the quantity $2\rho k/3$, to be consistent with (37); although this new term is generally dominated by the pressure itself, it is recommended to keep it when k can be estimated, as in the developments presented herein. One may also note that the conservation laws presented in Section 3 remain valid with the new momentum equation (40), since the mathematical form is unchanged in comparison to the laminar equation (10).

DOI: 10.1002/fld

The idea of Reynolds-averaging the SPH equations was presented by Violeau *et al*. [5] and Shao and Gotoh [9], using a mixing length turbulent closure. We present here a more sophisticated approach (see Reference [7]) based on the traditional k–ε model developed in the context of Eulerian numerical methods. Firstly, one defines for each particle a a turbulent kinetic energy k_a and an energy dissipation rate ε_a, and assumes the classical dimensional relation:

$$\nu_{T,a} = C_\mu \frac{k_a^2}{\varepsilon_a} \tag{42}$$

in which C_μ is an empirical constant [18]. Then, additional equations are required to calculate k_a and ε_a at each time step. The usual Lagrangian transport equation for turbulent kinetic energy takes the following continuous form:

$$\frac{\mathrm{d}k}{\mathrm{d}t} = P - \varepsilon + \nabla \cdot \left[\left(\nu + \frac{\nu_T}{\sigma_k} \right) \nabla k \right] \tag{43}$$

which is a scalar advection–diffusion equation similar to (35) (but in a continuous form), the production of kinetic energy P acting as a source term while the dissipation ε is a sink one [18]. Thus, in SPH formalism, a transport equation for k can be written in the following form:

$$\frac{\mathrm{d}k_a}{\mathrm{d}t} = P_a - \varepsilon_a + \sum_b m_b \frac{\mu_{k,a} + \mu_{k,b}}{\rho_a \rho_b} \frac{k_{ab}}{r_{ab}^2} \mathbf{r}_{ab} \cdot \nabla_a w_{ab} \tag{44}$$

where $\mu_{k,a} = \mu_a + \mu_{T,a}/\sigma_k$ is k's dynamic diffusivity. Equation (44) involves particle production P_a, turbulent diffusion (in which $k_{ab} = k_a - k_b$) and particle dissipation ε_a. As in usual turbulent diffusion models, the parameter σ_k is a Schmidt number defined as the ratio between the eddy viscosity and kinetic energy diffusivity. In continuous notations, the production term is defined by $P = -\mathbf{R} : \mathbf{S} = -R_{ij} S_{ij}$ (with Einstein's notation regarding i and j subscripts), giving together with (38)

$$P = \nu_T S^2 \tag{45}$$

with

$$S = \sqrt{2\mathbf{S} : \mathbf{S}} \tag{46}$$

referred to as the scalar mean rate-of-strain. However, in order to avoid any overestimation of k in case of large scalar rate-of-strain (as for instance in the case of impinging jet of breaking wave), one should keep in mind that turbulence anisotropy is always bounded by $C_\mu^{1/2}$ (see e.g. Reference [19]). Hence, we consider here a linear dependency on the rate-of-strain for large deformations, writing the production of particle a as

$$P_a = \min \left(\sqrt{C_\mu}, C_\mu S_a \frac{k_a}{\varepsilon_a} \right) k_a S_a \tag{47}$$

In order to estimate the scalar rate-of-strain S_a relative to particle a, velocity gradients appearing in (39) can be written in an SPH tensorial form as

$$\left(\frac{\partial \overline{u}_i}{\partial x_j} \mathbf{e}_i \otimes \mathbf{e}_j \right)_a = \rho_a \sum_b m_b \left(\frac{\overline{\mathbf{u}}_a}{\rho_a^2} + \frac{\overline{\mathbf{u}}_b}{\rho_b^2} \right) \otimes \nabla_a w_{ab} \tag{48}$$

DOI: 10.1002/fld

where $\mathbf{e}_i$ is the unit vector corresponding to the ith co-ordinate. Then, S_a can easily be computed from (46). However, this method implies an SPH interpolation in the form (48) for each pair of subscripts i and j, i.e. nine interpolations in 3D, which is not computationally efficient. Alternatively, one can come back to the continuous definition of energy dissipation for a viscous fluid, writing:

$$\frac{\mathrm{d}E}{\mathrm{d}t} = -\int_\Omega \rho \nu s^2 \,\mathrm{d}\Omega \tag{49}$$

in which s is the scalar rate-of-strain based on true velocities (instead of averaged ones). Thus, coming back to (25), (32) and (34) and approximating the integral appearing in (49) with the SPH interpolant (2), one obtains

$$\frac{1}{2}\sum_{a,b} \alpha_{ab}\mathbf{u}_{ab}^2 = \sum_a m_a \nu_a s_a^2 \tag{50}$$

This equation suggests an SPH form for s_a:

$$s_a^2 = \frac{1}{2\nu_a m_a}\sum_b \alpha_{ab}\mathbf{u}_{ab}^2 \tag{51}$$

Eventually, considering the definition (33) for the α_{ab}'s and coming back to averaged notations, we get

$$S_a^2 = -\frac{1}{2}\sum_b m_b \frac{\rho_a + \rho_b}{\rho_a \rho_b}\frac{\overline{u}_{ab}^2}{r_{ab}^2}\mathbf{r}_{ab}\cdot\nabla_a w_{ab} \tag{52}$$

where $\overline{u}_{ab} = |\overline{\mathbf{u}}_{ab}|$. Equation (52), based on a single interpolation, will be preferably used in the following. Note that the right-hand side of (52) is always positive, since $\nabla_a w_{ab}\cdot\mathbf{r}_{ab}$ is negative.

In the SPH k–ε model, (44) is integrated in time to calculate k_a using a temporal numerical scheme as for Equation (10). The dissipation rate ε can be similarly calculated, solving a new equation written in SPH language as

$$\frac{\mathrm{d}\varepsilon_a}{\mathrm{d}t} = \frac{\varepsilon_a}{k_a}(C_{\varepsilon,1}P_a - C_{\varepsilon,2}\varepsilon_a) + \sum_b m_b \frac{\mu_{\varepsilon,a} + \mu_{\varepsilon,b}}{\rho_a \rho_b}\frac{\varepsilon_{ab}}{r_{ab}^2}\mathbf{r}_{ab}\cdot\nabla_a w_{ab} \tag{53}$$

with $\mu_{\varepsilon,a} = \mu_a + \mu_{T,a}/\sigma_\varepsilon$. and $\varepsilon_{ab} = \varepsilon_a - \varepsilon_b$. Equation (53) is an SPH form of the traditional advection–diffusion equation for the dissipation rate [18]. Alternatively, the dissipation can be estimated from a dimensional relation like

$$\varepsilon_a = C_\mu^{3/4}\frac{k_a^{3/2}}{L_{m,a}} \tag{54}$$

where $L_{m,a}$ is a mixing length attached to particle a, which can be proportional to the particle size, or alternatively defined as a function of particle position for simple shear flows. In contrast to Equation (53), model (54) (here referred to as k–L_m) does not need any numerical scheme for ε; on the other hand, it requires the definition of a mixing length. Moreover, it has been shown in the past that the use of a differential equation for estimating ε gives much better results, and this is also true in the SPH context (see Section 7).

Both k and ε equations in SPH forms (44) and (53) satisfy the conservation properties mentioned in Section 3; in other terms, the diffusion terms are not responsible for any artificial energy loss,

DOI: 10.1002/fld

only contributing to the spatial re-distribution of k and ε in time through appropriate fluxes between particles. We use here the set of constant values recommended by Launder and Spalding [18]: $C_\mu = 0.09$, $\sigma_k = 1.0$, $\sigma_\varepsilon = 1.3$, $C_{\varepsilon,1} = 1.44$ and $C_{\varepsilon,2} = 1.92$. Dirichlet wall boundary conditions for kinetic energy and mean velocity are specified as

$$\begin{aligned} k_a &= \frac{u_{*,a}^2}{\sqrt{C_\mu}} \\ \frac{\overline{u}_a}{u_{*,a}} &= \frac{1}{\kappa} \ln \frac{\delta u_{*,a}}{v_a} + 5.2 \end{aligned} \tag{55}$$

for all particles located on solid boundaries (wall particles only). In the traditional log-law appearing in (55), $\kappa = 0.41$ is von Karman's constant, while $u_{*,a}$ is the shear velocity relative to wall particle a and v_a its molecular kinematic viscosity. δ is a distance arbitrarily chosen small enough in comparison to the particle size, but larger than the viscous sub-layer thickness. Note that a rough log-law for near-wall velocities can be easily programmed as a wall function in place of the smooth one (55). Eventually, the value of shear velocity attached to a wall particle can be estimated from the wall velocity gradient given by (48). In the k–ε SPH model, a Neumann wall condition for ε is enforced by setting the diffusion term appearing in (53) as $u_*^4/\sigma_\varepsilon \delta^2$ for all wall particles. However, this specific wall condition breaks conservativity for ε diffusion; indeed, prescribing a consistent Neumann boundary condition seems difficult, since ε presents a very high gradient near the wall. The use of symmetry based on mirror particles as we presented in Section 2 for density and pressure is thus unefficient in the case of ε.

Specific free-surface boundary conditions are not considered here, provided the lack of particles in the vicinity of a free surface makes all quantities rapidly decreasing when approaching the surface (as for pressure), which is enough for numerical stability and physical meaning. In particular, pressure, eddy viscosity and turbulent kinetic energy vanish near the free surface. A more accurate approach would require further investigation; however, since SPH was designed to treat complicated flows, identifying the particles located on the free surface seems not always straightforward.

An example of SPH turbulent computation in a 2D steady periodic (i.e. 'infinite') open-channel flow using the above-mentioned equations, is briefly presented in Figure 5. The water depth is $H = 0.4\,\mathrm{m}$ and the computation involves 40×40 fluid particles driven by a horizontal force

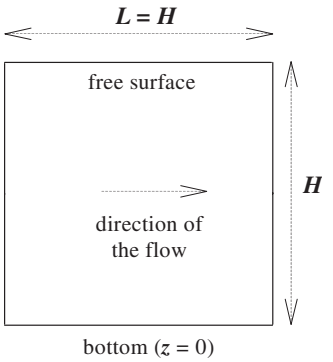

Figure 5. Sketch of the open-channel.

DOI: 10.1002/fld

playing the role of the pressure gradient resulting from a bed slope. We consider here a wall with roughness of 0.01 m. The bulk velocity is 0.753 m/s, giving a Reynolds number of 301 200 and a shear velocity of 0.05 m/s. Following Nezu and Nakagawa [20], the mixing length was defined as

$$L_{m,a} = \kappa z_a \sqrt{1 - \frac{z_a}{H}} \tag{56}$$

where z_a is the particle distance to the bed level. For this particular case, where the water depth is constant and thus the free-surface steady, a free-surface condition for energy dissipation was prescribed following [20], as $\varepsilon_a = k_a^{3/2}/\alpha H$ with $\alpha = 0.18$. Turbulent kinetic energy, dissipation rate, eddy viscosity and horizontal Reynolds-averaged velocities are compared to experimental and numerical data from References [20, 21], showing a fairly good agreement (Figure 6). In

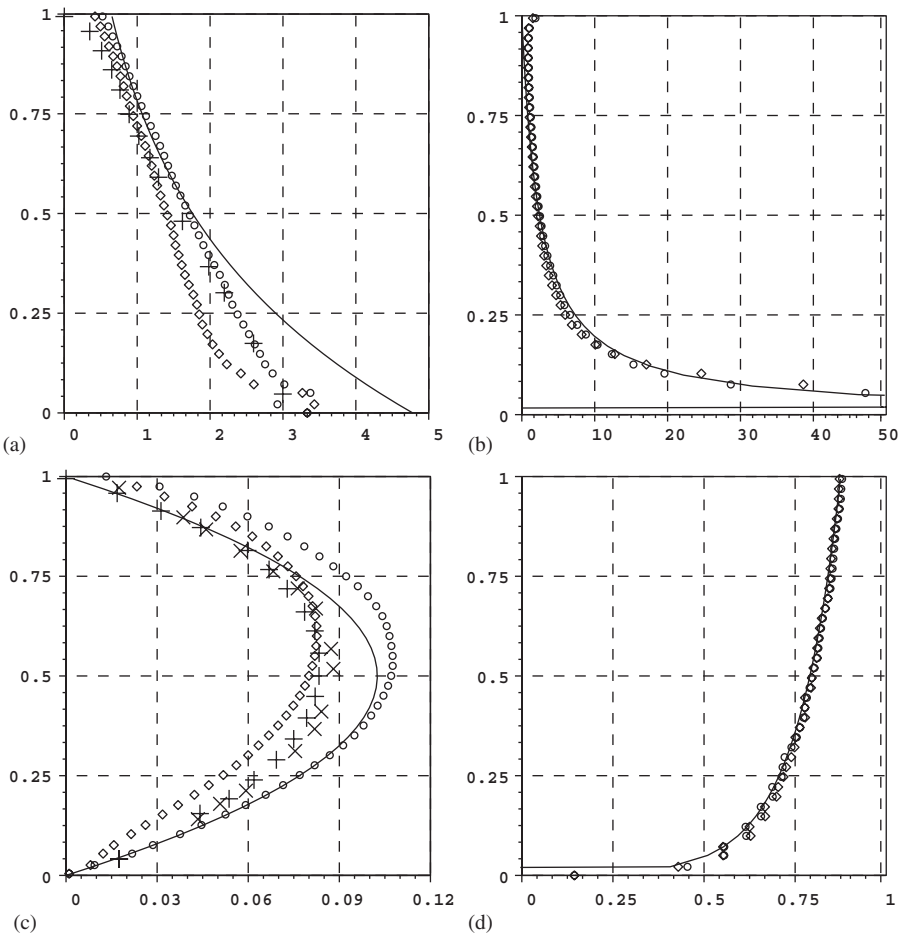

Figure 6. Open-channel turbulent steady flow. Distributions of: (a) k/u^2; (b) $\varepsilon H/u_*^3$; (c) ν_T/Hu_*; and (d) axial velocity in m/s versus non-dimensional distance to the bed z/H (on vertical axis). Present SPH method with ○ k–L_m model and ◊ k–ε model; — semi-empirical [20]; × experimental [20]; + finite elements k–ε [21].

DOI: 10.1002/fld

particular, the well-known velocity log-profile is correctly reproduced by the model. However, the wall Neumann condition regarding ε sometimes leads to underestimations of the eddy viscosity in the k–ε case. The reader can refer to References [6, 7] for more details about this test case. Despite its simplicity, it shows the ability of the proposed SPH k–ε model to predict the flow and averaged turbulent characteristic near a wall under permanent conditions. It also proves that the wall boundary conditions are correctly specified.

6. COLLAPSE OF A WATER COLUMN

Equations corresponding to the k–ε SPH model presented in the previous section are solved here in the case of a collapse of a 2 m high 2D water column in a tank, due to the gravity. The complete description of the experimental case is given by Koshizuka and Oka [22], and a brief sketch is given in Figure 7. The initial width of the column is $a = 1$ m and its height $2a$, while the tank is 4 m long, and the flow involves 20 000 fluid particles. Figure 8 presents distributions of velocity amplitude at different stages during this flow, showing a wave breaking. It must be emphasized that the k–ε turbulent closure, by providing a physical distribution of eddy viscosity in space, gives much smoother velocity and pressure fields than traditional SPH viscous models based on a constant (and sometimes artificial) viscosity, and thus increases the numerical stability of the method. Numerical tests have shown that a constant viscosity can even reach to numerical breakdown in the presented case.

From a qualitative point of view, the flow appears realistic; in particular, the treatment of solid walls seems satisfactory, although the particles positions are slightly scattered in the vicinity of the lower wall (see Figure 9). Figure 10 provides a quantitative validation of the model, showing the maximum x-position of the front and water depth on the left vertical wall. Comparison with experiments conducted in Reference [22] reveal a satisfactory agreement.

The present example shows that the proposed SPH k–ε model can treat complex flows involving highly disturbed free surfaces and rapid motion. However, no validation can be done

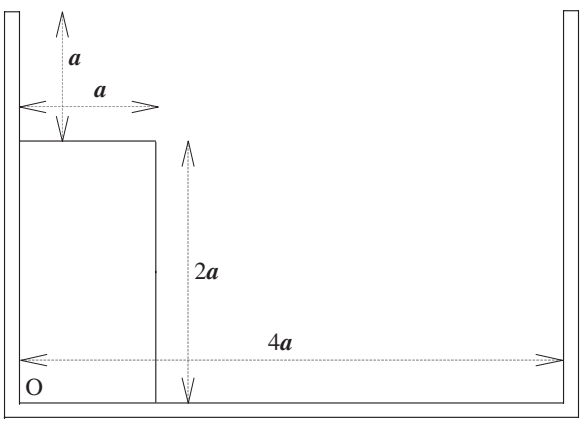

Figure 7. Sketch of the initial configuration of the water column.

DOI: 10.1002/fld

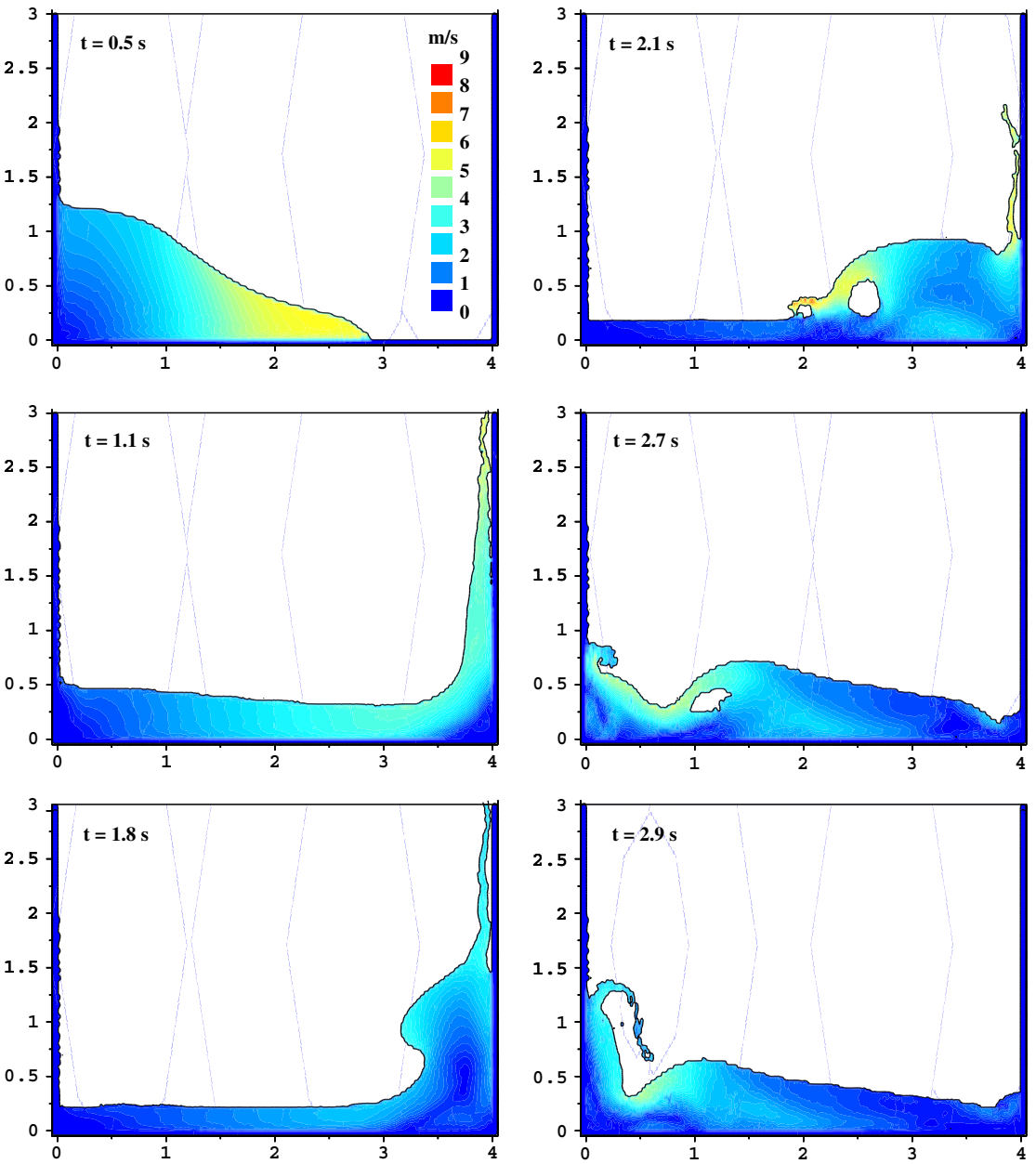

Figure 8. Collapse of a water column in a tank simulated with the present SPH k–ε model. Velocity magnitude distribution at various stages (the legend applies to all the snapshots). To clarify the visualization, the fields were interpolated on a spatial grid (not involved in the SPH computation). Distances are in metres.

DOI: 10.1002/fld

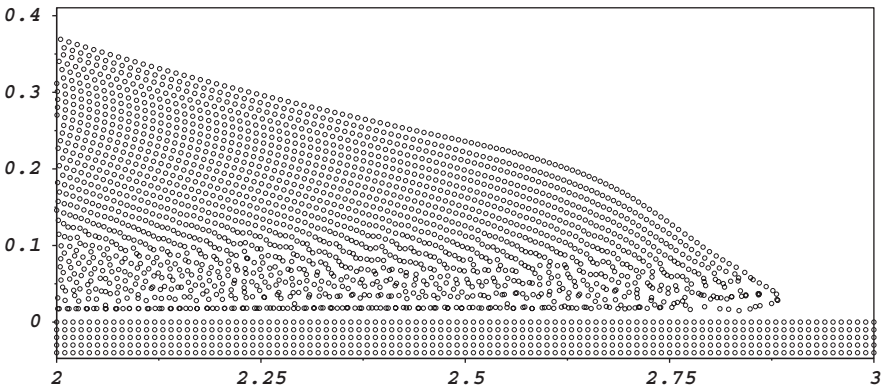

Figure 9. Collapse of a water column in a tank simulated with the present SPH k–ε model. Zoom on the particle positions near the wave front at $t = 0.5$ s (axis are labelled in metres).

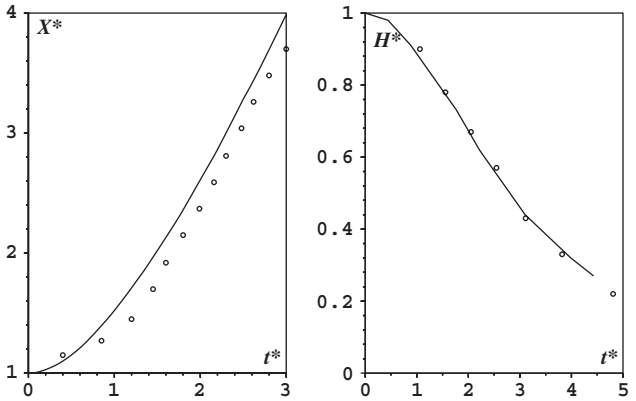

Figure 10. Collapse of a water column in a tank simulated with the present SPH k–ε model (solid lines). Non-dimensional maximum x-position $X^* = X/a$ and water depth $H^* = H/(2a)$ versus non-dimensional time $t^* = t(a/2g)^{1/2}$ (a is the initial column width). Validation with experiments (circles) from Reference [22].

in terms of shape of the free surface, which is of a great interest for all possible applications in environmental fluid mechanics. For example, estimating wave breaking is of major importance in coastal engineering, and the design of sea defence requires the prediction of wave run-up and overtopping. Both phenomena cannot be properly modelled without an appropriate prediction of the free surface in space and time. The next section will clarify this point and show that a more complicated approach is necessary for such a purpose.

7. EXPLICIT ALGREBRAIC REYNOLDS STRESS MODELS

Despite its ability to correctly simulate complex flows, the k–ε model was proved to be inaccurate when modelling violent distortions, or more generally non-isotropic flows, in which the largest

DOI: 10.1002/fld

turbulent eddies can exhibit a complex behaviour involving non-linear dependency on boundary conditions (see e.g. Reference [23]). A more accurate approach, still based on a Reynolds-averaging idea, was first proposed by Pope [24] for two-dimensional flows, then extended by Gatski and Speziale [25] to three dimensions. However, in the following we will refer to Reference [26]. Referred to as 'EARSM', these closure forms consist of setting Reynolds stresses through an explicit dependency upon the rate-of-strain and vorticity tensors components as

$$\mathbf{R}=\frac{2}{3}k\mathbf{I}-2C_\mu\frac{k^2}{\varepsilon}\left[\mathbf{S}+C_2\frac{k}{\varepsilon}(\mathbf{S\Omega}-\mathbf{\Omega S})\right] \tag{57}$$

where $\mathbf{S}$'s components are defined by (39), while the components of the vorticity (or rotation rate) tensor $\mathbf{\Omega}$ are

$$\Omega_{ij}=\frac{1}{2}\left(\frac{\partial\overline{u}_i}{\partial x_j}-\frac{\partial\overline{u}_j}{\partial x_i}\right) \tag{58}$$

One should emphasize the fact that model (57) is only valid in two dimensions; we will then reduce our considerations to this case in the present section. If the constant C_2 was zero, the above equation would simply give Boussinesq's model (38) with an eddy viscosity specified by (42), in which there is no dependency on $\mathbf{\Omega}$. The additional terms presented in (57) hence model the possible effects of mean flow rotation, but also non-linear strain dependency. In the form presented here, the coefficients C_μ and C_2 are defined by

$$\begin{aligned}C_\mu&=\frac{B_3}{2}\frac{P^*+B_0}{(P^*+B_0)^2+(B_2\Omega^*)^2}\\ C_2&=\frac{B_2}{P^*+B_0}\end{aligned} \tag{59}$$

where $P^*=P/\varepsilon$ is the production-to-dissipation ratio and $\Omega^*=k\Omega/\varepsilon$, where $\Omega^2=2\mathbf{\Omega}:\mathbf{\Omega}$ is the scalar mean rotation rate (squared). The model constants are $B_0=0.8$, $B_2=\frac{4}{9}$ and $B_3=\frac{8}{15}$. One can see that C_μ is no longer a constant but depends on the production (among other variables). The production rate, as defined by $P=-\mathbf{R}:\mathbf{S}$, is thus more complicated than the simple formulae (45) and (47) used in traditional Boussinesq-type models, and also depends on Ω. The explicit dependency is given by the following third-order polynomial equation:

$$P^{*3}+2B_0P^{*2}-\left(\frac{B_3}{2}S^{*2}-B_2^2\Omega^{*2}-B_0^2\right)P^*-\frac{B_0B_3}{2}S^{*2}=0 \tag{60}$$

with $S^*=kS/\varepsilon$. Solution to (60), discussed in Reference [26], becomes linear in S^* for large strain in the particular case of a shear flow (i.e. $\Omega=S$), as previously suggested by Equation (47). A second consequence of the variability of C_μ should be the explicit dependency of the eddy viscosity on production through (42). However, it is known that accounting for such a dependency often yields numerical instabilities [27]; therefore we considered in (42)—and thus in (57)—a traditional constant value of 0.09 for C_μ.

Modelling turbulence with the EARSM then consists of solving the RANS momentum equation (37) with Reynolds stresses defined by (57). A possible SPH form for the stress divergence applied

DOI: 10.1002/fld

to particle a is

$$\left[\frac{1}{\rho}\nabla\cdot(\rho\mathbf{R})\right]_a=\sum_b m_b\left(\frac{\mathbf{R}_a}{\rho_a}+\frac{\mathbf{R}_b}{\rho_b}\right)\cdot\nabla_a w_{ab} \tag{61}$$

It should be used in place of the SPH turbulent viscous term in (40). In the form (61), SPH Reynolds forces present the linear momentum conservation property already mentioned in part 3; however, conservation of angular momentum is generally broken. Although some authors (see e.g. Reference [28]) use a form like (61) to model viscous forces, it is known to be rather sensitive to particle disorder. Hence, in the present work we suggest to replace (61) with an additional SPH-viscous term in the momentum equation, to yield

$$\frac{\mathrm{d}\overline{\mathbf{u}}_a}{\mathrm{d}t}=-\sum_b m_b\left[\left(\frac{\overline{p}_a}{\rho_a^2}+\frac{\overline{p}_b}{\rho_b^2}-\frac{\mu_{e,a}+\mu_{e,b}}{\rho_a\rho_b}\frac{\overline{\mathbf{u}}_{ab}}{r_{ab}^2}\mathbf{r}_{ab}\cdot\right)\nabla_a w_{ab}-\widetilde{\mathbf{\Pi}}_{ab}\right]+\mathbf{g} \tag{62}$$

The new viscous term $\widetilde{\mathbf{\Pi}}_{ab}$ is an SPH approximation of the divergence of the non-linear term involving $\mathbf{S\Omega}-\mathbf{\Omega S}$ in (57), and is defined as

$$\widetilde{\mathbf{\Pi}}_{ab}=-\frac{\widetilde{\mu}_{T,a}+\widetilde{\mu}_{T,b}}{\rho_a\rho_b}\frac{\boldsymbol{\omega}\overline{\mathbf{u}}_{ab}}{r_{ab}^2}\mathbf{r}_{ab}\cdot\nabla_a w_{ab} \tag{63}$$

$\widetilde{\mu}_{T,a}$ being a non-linear eddy viscosity given by

$$\widetilde{\mu}_{T,a}=C_{2,a}\frac{k_a\Omega_a}{\varepsilon_a}\mu_{T,a} \tag{64}$$

(one should keep in mind that C_2, defined by (59), is *not* a constant and thus should be calculated for each particle), and $\boldsymbol{\omega}$ a 2D constant second-order tensor playing the role of a 'rotation unit tensor':

$$\boldsymbol{\omega}=\begin{pmatrix}0 & 1\\ -1 & 0\end{pmatrix} \tag{65}$$

With the model presented above, the total viscous SPH force (involving $\mathbf{\Pi}_{ab}+\widetilde{\mathbf{\Pi}}_{ab}$) is in the generic form (24)—except that we now have averaged velocities, with

$$\mathbf{A}_{ab}=-\frac{m_a m_b}{\rho_a\rho_b}\frac{\mathbf{r}_{ab}\cdot\nabla_a w_{ab}}{r_{ab}^2}(\mathbf{M}_a+\mathbf{M}_b) \tag{66}$$

an eddy viscosity tensor $\mathbf{M}_a$ being now defined for all particles as

$$\mathbf{M}_a=\mu_{e,a}\mathbf{I}-\widetilde{\mu}_{T,a}\boldsymbol{\omega} \tag{67}$$

The non-linear viscous term (67) no longer vanishes for a rigid body rotation, because of the $\boldsymbol{\omega}$ tensor. However, the definition of $\boldsymbol{\omega}$, together with (25) and (34), shows that it does not generate any additional mean-flow energy dissipation; the new viscous term thus redistributes kinetic energy in a different manner. Note that, although we refer to the linear model (24), model (63) contains a non-linearity in the terms like $\widetilde{\mu}_{T,a}\overline{\mathbf{u}}_{ab}$, thus involving $\Omega_a\overline{\mathbf{u}}_{ab}$ through the definition (64) of the non-linear viscosity. Equations (44) and (53) are still needed to calculate k_a and ε_a, both required in (57) and (59). The rotation rate Ω_a of particle a may be estimated from its definition (58)

DOI: 10.1002/fld

through equation (48) for the calculation of the rate-of-strain components. An interesting feature of EARSM, particularly in the SPH context, is that no wall boundary condition is required for R_{ij}, Reynolds stresses being prescribed everywhere from (57). Boundary conditions regarding k and ε are unchanged.

An EARSM seems not particularly interesting in the simple case of shear flows like the open-channel presented at the end of Section 5, since the presented model is designed to provide the same results as k–ε for simple shear flows. However, even in such an elementary flow, EARSM provide better results, as it can be seen in Figure 11; in particular, the vertical distribution of turbulent kinetic energy is improved in comparison to the k–ε results presented in Figure 6. Numerical tests have shown that, in this particular case, the progress is mainly due to the corrected definition of production rate by Equation (60). Indeed, in the vicinity of the channel bed, the non-dimensional strain S^* is slightly smaller than the equilibrium value of $C_\mu^{-1/2} = 3.33$ predicted

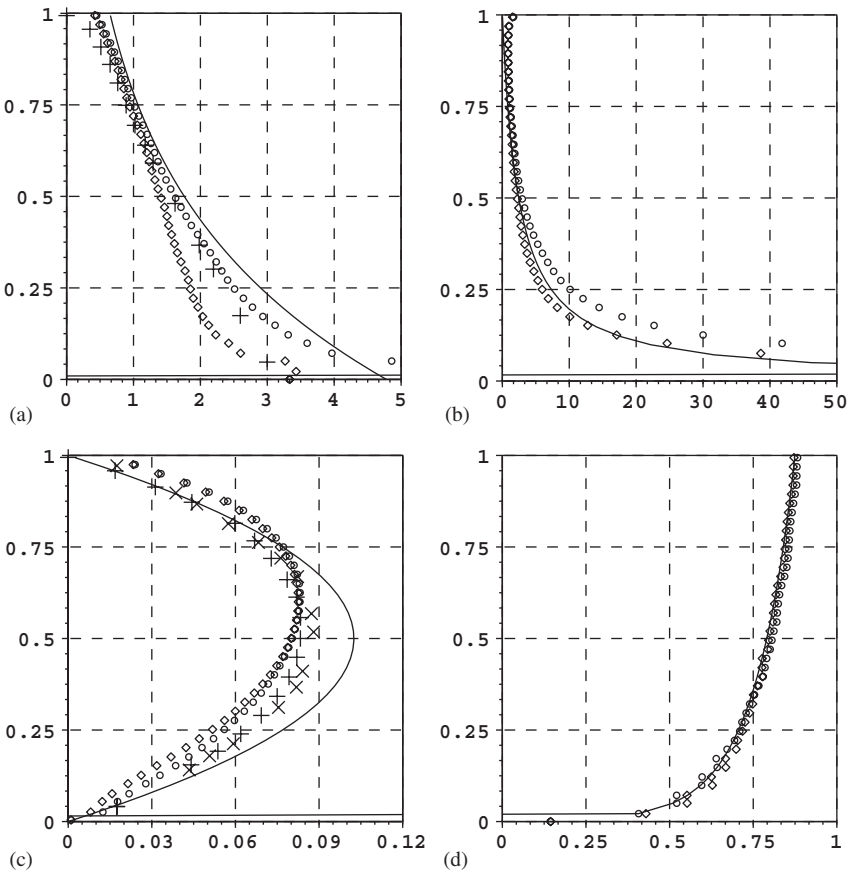

Figure 11. Open-channel turbulent steady flow. Vertical distributions of: (a) k/u_*^2; (b) $\varepsilon H/u_*^3$; (c) ν_T/Hu_*; and (d) axial velocity in m/s versus non-dimensional distance to the bed. Present SPH method with ○ EARSM and ◊ linear k–ε model; — semi-empirical [20]; × experimental [20]; + finite elements k–ε [21].

DOI: 10.1002/fld

by the standard theory of log-layers; as a consequence the ratio of production to dissipation P^* is slightly underestimated with traditional models (45) and (47), while (60) provides the correct amount of turbulent kinetic energy near the bed, which then diffuses into the water column. As a consequence, eddy viscosity is also slightly better predicted near the bed.

The collapse of a water column shown in Section 6 is so complex that traditional models like linear k–ε should be insufficient for an accurate description of velocity fields and free-surface shape. At the wave breaking point, strain is rather high and vorticity appears, involving non-linear terms in Reynolds stresses. A smaller water column was simulated with k–L_m, linear k–ε and EARSM, then compared with a laboratory experiment. Even with such an elementary comparison, Figure 12 shows that increasing the turbulence closure complexity significantly improves the accuracy of the free-surface prediction, as required. In particular, it can be seen that the non-linear viscosity, increasing diffusion, is capable of predicting the correct behaviour of wave breaking. Hence, we suspect that a correct modeling of complex wave motion (breaking, overtopping of a coastal dyke) could not be done without a sophisticated turbulence closure. However, the free-surface location from experimental pictures is too rough to draw out solid conclusions about the real accuracy of the model. Thus, despite these encouraging features, the present model would require a more accurate and systematic validation; the EARSM SPH model will be presented in further details in a later publication.

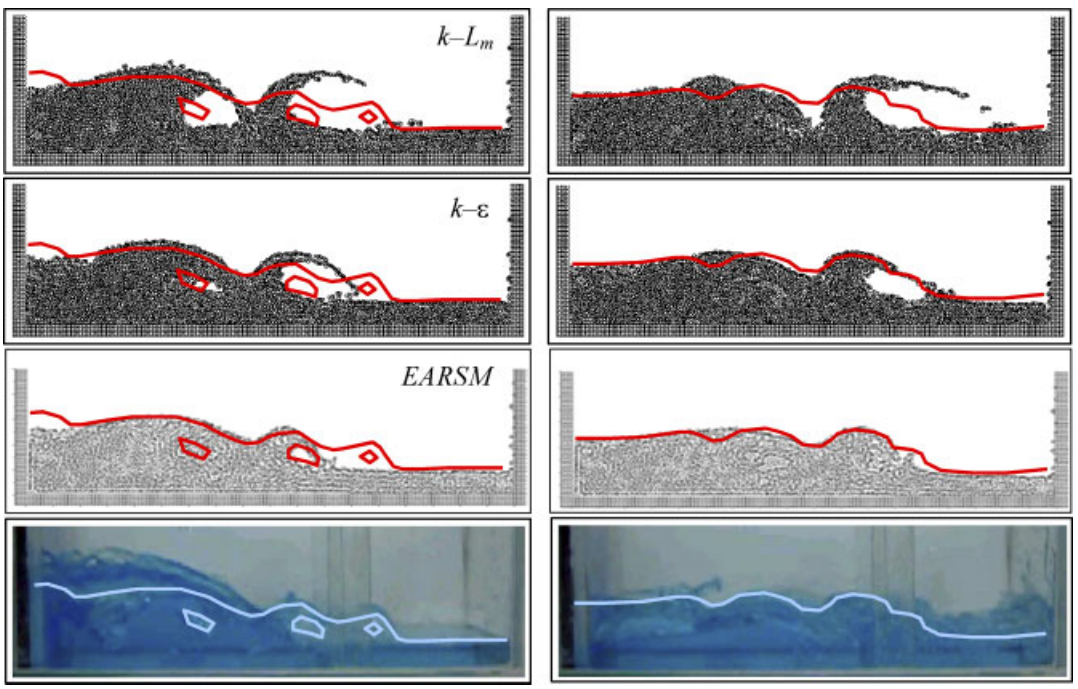

Figure 12. Collapse of a water column simulated with present SPH model and observed in a real tank at two stages (left column: $t = 1.02$ s; right column: $t = 1.10$ s). From top to bottom: k–L_m, linear k–ε and EARSM SPH models, experiments. The shape of the experimental free surface (projected on the front glass) is approximately shown with solid lines; one should not consider three-dimensional perspective for this comparison with the 2D-model.

DOI: 10.1002/fld

8. 3D LARGE EDDY SIMULATION

Despite its accuracy, the EARSM described in the previous section is somewhat complex and is still based on Reynolds-averaged values. Alternatively, LES, now recognized as a key tool for turbulence modelling (see e.g. Reference [23]), provides much more detailed information on the turbulence itself and is more suitable for far-from-equilibrium flows, while considering reasonable computational costs (whereas in the particular of the SPH method, the coast can be high; this will be discussed later). The main idea of LES is to simulate the large scales of turbulent motions while modelling the dissipative effect of smaller ones. This is justified by the fact that large scales carry the main part of turbulent kinetic energy and are most likely anisotropic whereas small scales are believed to be almost isotropic. It is hence essential to define modified fields that only contain the large-scale components of instantaneous fields. In the context of Eulerian methods, each true flow variable A is thus decomposed into a large-scale component $\widetilde{A}$ and a small scale (or subgrid scale) component A' such as $A = \widetilde{A} + A'$, where $\widetilde{A}$ is defined by the following filtering operator:

$$\widetilde{A}(\mathbf{r}) = \int_{\Omega} A(\mathbf{r}')G_{\Delta}(\mathbf{r} - \mathbf{r}')\,\mathrm{d}r' \tag{68}$$

where G_{Δ} is a filter function depending on the separation between spatial locations. Coming back to SPH, one can firstly notice that Equation (68), from a formalistic point of view, is very similar to the basic SPH relation (1): the kernel function is analogous to the filter function and the smoothing length h is equivalent to the filter size Δ. Thus, one can define an SPH filtered quantity $\widetilde{A}$ as

$$\widetilde{A}_a = \sum_b \frac{m_b}{\rho_b} A_b w_{ab} \tag{69}$$

When filtering the continuous Navier–Stokes equations, one obtains a set of equations very similar in form to the RANS equations, with averaged values replaced by filtered ones and the Reynolds stress tensor changed with a subgrid (here, sub-particle) scale one, representing the contribution of small scales (i.e. turbulent structures smaller than the particle size) on larger scales. When modelling this tensor through a sub-particle eddy viscosity assumption, the filtered Navier–Stokes equations are identical to the eddy-viscosity RANS equations, from a formalistic point of view. In SPH formalism, according to the above-mentioned similarity between the Reynolds-averaged and filtered Navier–Stokes equations, they are hence written as

$$\frac{\mathrm{d}\widetilde{\mathbf{u}}_a}{\mathrm{d}t} = -\sum_b m_b \left(\frac{\widetilde{p}_a}{\rho_a^2} + \frac{\widetilde{p}_b}{\rho_b^2} - \frac{\mu_{S,a} + \mu_{S,b}}{\rho_a \rho_b} \frac{\widetilde{\mathbf{u}}_{ab}}{r_{ab}^2} \mathbf{r}_{ab} \cdot \right) \nabla_a w_{ab} + \mathbf{g} \tag{70}$$

$$\frac{\mathrm{d}\rho_a}{\mathrm{d}t} = \sum_b m_b \widetilde{\mathbf{u}}_{ab} \cdot \nabla_a w_{ab} \tag{71}$$

in analogy with (58), with $\rho_a \approx \widetilde{\rho}_a$ (since the fluid is nearly incompressible) and $\widetilde{\mathbf{u}}_{ab} = \widetilde{\mathbf{u}}_a - \widetilde{\mathbf{u}}_b$. The filtered pressure $\widetilde{p}_a$ is once again calculated from the density by the state equation (14). The sub-particle eddy viscosity of particle a $\mu_{S,a} = \rho_a \nu_{S,a}$ can be modelled by the following SPH Smagorinsky model:

$$\nu_{S,a} = (C_S h)^2 \sqrt{2\widetilde{\mathbf{s}}_a : \widetilde{\mathbf{s}}_a} \tag{72}$$

where $\widetilde{\mathbf{s}}_a$ denotes the filtered rate-of-strain tensor associated to particle a, thus defined from Equation (39) with filtered velocities in place of Reynolds-averaged ones; hence a formula like

DOI: 10.1002/fld

(52) can still be used in this context. C_S is the Smagorinsky constant usually close to 0.15 [23], and h is the smoothing length (or alternatively initial particle spacing), playing here the role of a constant numerical mixing scale.

Despite its apparent simplicity, in contrast to traditional RANS models presented in previous sections, LES must always be done in three dimensions (since turbulent structures are essentially three dimensional) and results need to be averaged for industrial use, which requires substantially more computational time. This SPH Smagorinski model was implemented in a 3D SPH code and tested in a turbulent open-channel flow similar to the case described in Section 5, with different size and flow features. The canal is 1.2 m long, 0.2 m wide and 0.4 m high and contains 100 000 fluid particles. The bulk velocity is 1.345 m/s, leading to a Reynolds number of 538 000. The left picture of Figure 13 presents an instantaneous field of velocity magnitude; one can notice that it is typically turbulent, with velocity fluctuations in all directions. However, the numerical fluctuating motion inherent to the Lagrangian basis of SPH, which behaves like a Monte-Carlo method even in laminar flows, raises new challenges in terms of separating this numerical noise from real turbulent fluctuations, which needs further investigation. Nevertheless, the averaged axial velocity profile is consistent with the log-law, as shown on the right side of Figure 13 (time-averaging velocities can here be done since the mean flow is steady).

The model was also applied to a 3D collapse of water column similar to those presented in Section 7, with 120 000 fluid particles. The initial water box is 0.3 m high, 0.3 m long and 0.6 m wide, while the tank length is 0.9 m. Figure 14 shows instantaneous free-surface evolution, revealing a realistic breaking wave when compared to the experimental produced at the Technical University of Delft [6]. Further investigation is currently carried out to get information relative to turbulent parameters and average fields for the presented cases. More details about the presented SPH LES model can be found in References [6, 8]. Finally, one should mention that the three-dimensional SPH approach together with the LES model reaches to high computational costs, due to the numerous filtering operations like Equation (69). This makes detailed numerical investigation

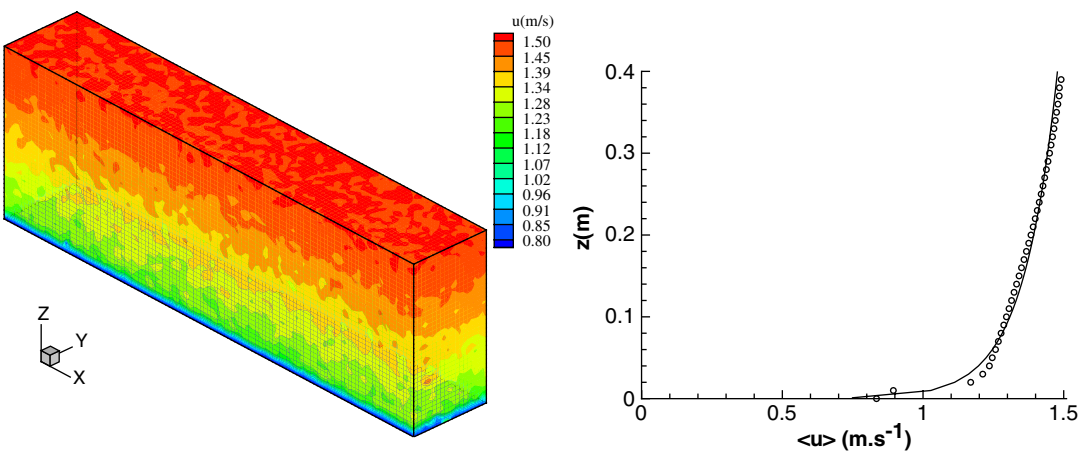

Figure 13. 3D turbulent open-channel flow simulated with the present SPH LES model. Left: 3D turbulent velocities. Right: vertical profile of averaged axial velocity; ○ present SPH method with LES model; — smooth bed log-law.

DOI: 10.1002/fld

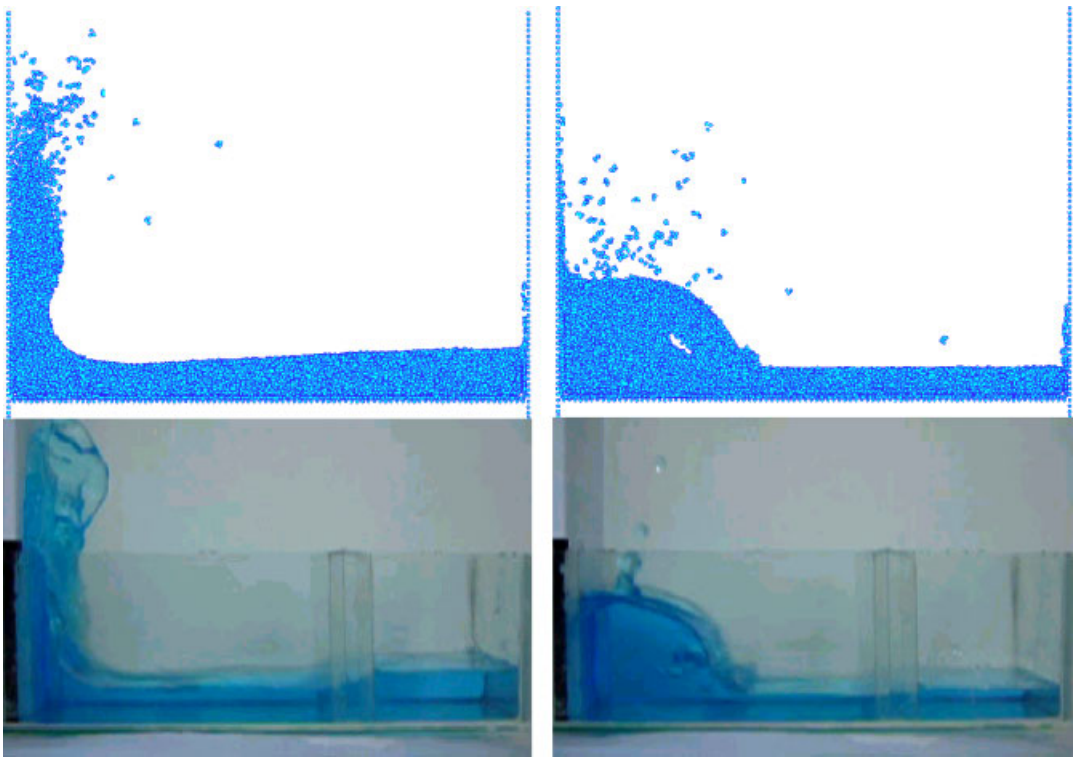

Figure 14. Collapse of a water column: comparison between present 3D SPH LES method and laboratory experiments [6] at two different stages: $t = 0.485$ s (left) and $t = 0.890$ s (right).

uneasy; further work on this subject will certainly need parallel algorithms. Thus, no definitive conclusions can be drawn regarding the possible use of LES in SPH for industrial or environmental applications.

9. CONCLUSIONS AND FUTURE WORK

From the above-mentioned applications, it appears that SPH is a very promising method for the simulation of complex turbulent flows involving distorted free surfaces in two or three dimensions. It may be emphasized that the developments presented herein do not cover all the possibilities of SPH in CFD: in particular, the method allows the modelling of floating bodies, fluid–structure interactions and two-phase flows. The developments made in Section 5 also tend to suggest that modelling turbulent scalar transport in SPH is a possible task. However, some drawbacks of the SPH method can easily be pointed out. The Courant condition appearing in (15) leads to rather small time steps, and the high number of particles required in 3D makes SPH a very computationally demanding method. The presented explicit weakly compressible scheme could also be criticized since it generally predicts scattered pressure fields. Some authors like Shao and

DOI: 10.1002/fld

Gotoh [9] have demonstrated the possibility of modelling truly incompressible flows with SPH, which is an alternative choice to increase the time step and provide smooth pressure fields under all circumstances.

The presented turbulence closure models, although not yet deeply validated in the case of complex free-surface flows, have shown to be attractive. Some of them (e.g. k–ε or LES), today considered as traditional in the context of Eulerian methods, have been proved to be adapted to the particular context of SPH and were applied with success on validated test cases. The merits of each model, in terms of accuracy and/or simplicity, partly appear from the presented simulations. For practical applications in CFD with SPH, it appears that the standard k–ε provides satisfactory results, while it can be inappropriate in the particular field of free-surface flows. The modelling of complex surfaces should be more successfully predicted with EARSM, to take account of strong distorsion and rotation effects. By highlighting the weaknesses of those turbulence closures in regards of the modelled flows, this work also suggests possible ways of improvements. Hence, future developments should be done around the problem of free surface and wall effects as well as associated boundary conditions.

LES was too briefly investigated here to draw definite conclusions. The high 3D computational time makes this approach especially cumbersome with SPH. Indeed, the use of SPH as an operational tool for three dimensional applications will require a parallelized code. Among other key points, further work will focus on this development. One may also mention that other appropriate and specific turbulent methods, like stochastic (pdf) models (see Reference [23]) were also tried in the context of SPH [5, 29] and may constitute a suitable alternative to LES to keep computational time reasonable.

In conclusions, the standard k–ε equations, here applied to SPH, are recommended for practical applications in industrial or environmental CFD with SPH. However, under specific circumstances, they should be inappropriate, in particular when modelling very complex free surface, where more advanced models should be used, like the proposed EARSM.

ACKNOWLEDGEMENTS

R. Issa acknowledges scientific guidance from Dr B. Boersma (TU Delft) and Prof. D. Laurence (UMIST Manchester), as well as financial support from the EU commission through a Marie Curie network (contract number HPMT-CT-01-00369) coordinated by Prof. C. Vassilicos (Imperial College of London) and Prof. F. T. M. Nieuwstadt (TU Delft).

REFERENCES

1. Gingold RA, Monaghan JJ. Kernel estimates as a basis for general particle methods in hydrodynamics. *Journal of Computational Physics* 1982; **46**:429–453.
2. Monaghan JJ. Smoothed particle hydrodynamics. *Annual Review of Astrophysics* 1992; **30**:543–574.
3. Gray JP, Monaghan JJ, Swift RP. SPH elastic dynamics. *Computer Methods in Applied Mechanics and Engineering* 2001; **190**:6641–6662.
4. Monaghan JJ. Simulating free surface flows with SPH. *Journal of Computational Physics* 1994; **110**:399–406.
5. Violeau D, Piccon S, Chabard JP. Two attempts of turbulence modelling in smoothed particle hydrodynamics. *Proceedings of the 8th Symposium on Flow Modelling and Turbulence Measurements*. Advances in Fluid Modelling and Turbulence Measurements. World Scientific: Singapore, 2002; 339–346.
6. Issa R. Numerical assessment of the smoothed particle hydrodynamics gridless method for incompressible flows and its extension to turbulent flows. *Ph.D. Thesis Report*, Department of Mechanical, Aerospace and Manufacturing Engineering, University of Manchester, U.K., 2005.

DOI: 10.1002/fld

7. Violeau D. One and two-equations turbulent closures for smoothed particle hydrodynamics. *Proceedings of the 6th International Conference on Hydroinformatics.* World Scientific: Singapore, 2004; 87–94.
8. Issa R, Violeau D, Laurence D. A first attempt to adapt 3D large eddy simulation to the Smoothed Particle Hydrodynamics gridless method. *Proceedings of the International Conference on Computational and Experimental Engineering and Sciences*, *1st Symposium on Meshless Methods*, Stara-Lesna, Slovaquia, 2005, in press.
9. Shao S, Gotoh H. Simulating coupled motion of progressive wave and floating curtain wall by SPH-LES model. *Coastal Engineering Journal* 2004; **46**:171–202.
10. Dalrymple RA, Rogers BD. Numerical modeling of water waves with the SPH method. *Coastal Engineering* 2006; **53**:141–147.
11. Morris JP, Fox PJ, Zhu Y. Modelling low Reynolds number incompressible flows using SPH. *Journal of Computational Physics* 1997; **136**:214–226.
12. Landau LD, Lifchitz EM. *Theoretical Physics*, *Mechanics*. Mir: Moscow, 1989.
13. Bonet J, Lok T-SL. Variational and momentum preservation aspects of smoothed particle hydrodynamics formulations. *Computational Methods in Applied Mechanics and Engineering* 1999; **180**:97–115.
14. Landau LD, Lifchitz EM. *Theoretical Physics*, *Statistical Physics*. Mir: Moscow, 1967.
15. Cleary PW, Monaghan JJ. Conduction modelling using smoothed particle hydrodynamics. *Journal of Computational Physics* 1999; **148**:227–264.
16. Uribe JC, Laurence D. *10th Ercoftac* (*SIG15*)/*IAHR*/*QNET-CFD Workshop on Refined Turbulence Modelling*, 2000.
17. Issa R, Lee E-S, Violeau D, Laurence D. Incompressible separated flows simulations with the smoothed particle hydrodynamics gridless method. *International Journal for Numerical Methods in Fluids* 2004; **47**:1101–1106.
18. Launder BE, Spalding DB. *Mathematical Models of Turbulence*. Academic Press: London, 1972.
19. Guimet V, Laurence D. A linearised turbulent production in the k–ε model for engineering applications. *Proceedings of the 5th International Symposium on Engineering Turbulence Modelling and Measurements*, Mallorca, 2002.
20. Nezu I, Nakagawa H. Turbulence in open-channel flows. *IAHR Monograph*, 1993.
21. Warner JC, Sherwood CR, Arango HG, Signell RP. Performance of four turbulence closure models implemented using a generic length scale method. *Ocean Modelling* 2005; **8**:81–113.
22. Koshizuka S, Oka Y. Moving-particle semi-implicit method for fragmentation of compressible fluid. *Nuclear Science Engineering* 1996; **123**:421–434.
23. Pope SB. *Turbulent Flows*. Cambridge University Press: Cambridge, MA, 2000.
24. Pope SB. A more general effective-viscosity hypothesis. *Journal of Fluid Mechanics* 1975; **2**:331–340.
25. Gatski TB, Speziale CG. On explicit algebraic stress models fox complex turbulent flows. *Journal of Fluid Mechanics* 1993; **254**:59–78.
26. Wallin N, Johansson AV. An explicit algebraic Reynolds stress model for incompressible and compressible turbulent flows. *Journal of Fluid Mechanics* 2000; **403**:89–132.
27. Rodi W. *Turbulence Models and their Applications in Hydraulics*. IAHR: Delft, 1980.
28. Speith R, Riffert H. The viscous gas ring as an astrophysical test problem for a viscous SPH-code. *Journal of Computational and Applied Mathematics* 1999; **109**:231–242.
29. Welton WC. Two-dimensional PDF/SPH simulations of compressible turbulent flows. *Journal of Computational Physics* 1998; **139**:410–443.

DOI: 10.1002/fld